Ultrafast Relaxation of Symmetry-Breaking Photo-Induced Atomic Forces

Shane M. O'Mahony,[1,2] Felipe Murphy-Armando,[2] Éamonn D. Murray,[3] José D. Querales-Flores,[2] Ivana Savić,[2] and Stephen Fahy[1,2]

[1]*Department of Physics, University College Cork, Cork T12K8AF, Ireland*

[2]*Tyndall National Institute, Cork T12R5CP, Ireland*

[3]*Department of Physics and Department of Materials, Imperial College London, London SW7 2AZ, United Kingdom*

(Received 22 March 2019; revised manuscript received 24 May 2019; published 23 August 2019)

We present a first-principles method for the calculation of the temperature-dependent relaxation of symmetry-breaking atomic driving forces in photoexcited systems. We calculate the phonon-assisted decay of the photoexcited force on the low-symmetry E_g mode following absorption of an ultrafast pulse in Bi, Sb, and As. The force decay lifetimes for Bi and Sb are of the order of 10 fs and in agreement with recent experiments, demonstrating that electron-phonon scattering is the primary mechanism relaxing the symmetry-breaking forces. Calculations for a range of absorbed photon energies suggest that larger amplitude, symmetry-breaking atomic motion may be induced by choosing a pump photon energy which maximizes the product of the initial E_g force and its lifetime. The high-symmetry A_{1g} force undergoes a partial decay to a nonzero constant on similar timescales, which has not yet been measured in experiments. The average imaginary part of the electron self-energy over the photoexcited carrier distribution provides a crude indication of the decay rate of symmetry-breaking forces.

DOI: 10.1103/PhysRevLett.123.087401

The generation and control of atomic forces in optically excited molecules and materials is important for a number of areas including photocatalysis [1], laser annealing, and the study of photoassisted phase transitions [2–4], with applications that include the development of efficient renewable energy [5] and phase-change memories [6,7]. The development of ultrafast optical spectroscopy has greatly advanced our understanding of electron and phonon dynamics in optically excited materials, with time resolution on the tens-of-femtoseconds scale readily accessible [8–10]. More recently, time-resolved x-ray diffraction and time-resolved photoemission spectroscopy have allowed the direct observation of atomic motion and electronic dynamics on timescales shorter than a picosecond following photoexcitation [11–14], providing insight into the physics of strongly correlated and charge density wave systems [15,16].

Photoexcitation with a laser pulse of duration much less than the fastest phonon period can be used to launch large amplitude coherent atomic motion in a variety of materials and molecules [11]. However, symmetry-breaking coherent atomic motion has been shown experimentally to have an amplitude orders of magnitude less than that of symmetry-preserving coherent atomic motion in a variety of materials [17–20]. Furthermore, the amplitudes of symmetry-breaking modes decrease strongly with increasing sample temperature, whereas high-symmetry mode amplitude is relatively insensitive to temperature, indicating very different aspects of the ultrafast dynamics affecting the two cases. If we understand the limiting mechanisms, it may be possible to suppress them and drive larger amplitude symmetry-breaking coherent atomic motion.

Bi and Sb are useful model systems for pump-probe reflectivity experiments due to their large vibrational response to optical excitation [21–24]. High-symmetry coherent A_{1g} phonons can be generated through a mechanism termed displacive excitation of coherent phonons (DECP) [25], related to the absorptive part of the Raman response [26]. When the pump pulse is polarized perpendicular to the threefold rotational axis of the crystal, the symmetry-breaking E_g mode has also been detected [12,17], but with a much lower and strongly temperature-dependent amplitude.

In this work, we provide for the first time a quantitative understanding of how incoherent electron-phonon scattering limits the generation of symmetry-breaking coherent atomic motion. We combine density functional perturbation theory (DFPT) [27], and electron-phonon scattering rate equations [28–30] to calculate the evolution on fs timescales of a photoexcited electronic distribution generated by optical absorption, and compute the resulting time-dependent atomic forces in the group-V semimetals, Bi, Sb, and As. We find that electron-phonon scattering dominates in determining the lifetime of the E_g driving force in photoexcited Bi and Sb, with calculated lifetimes in good agreement with recent experiments [17], and we predict similar behavior in As. We calculate the dependence of the initial atomic driving forces and their lifetimes on the photon energy of the pump pulse and suggest how variation

of the incident photon energy may be used to maximize the impact on low-symmetry atomic motion.

Our method goes beyond standard time-dependent density functional theory (TDDFT) [31] approaches by explicitly considering the coupling of the excited electron-hole plasma to the continuum of thermal phonon modes throughout the Brillouin zone and can be used to compute the lifetime of symmetry-breaking photoinduced atomic forces on ultrafast timescales in a variety of materials.

At room temperature, the E_g mode in bismuth (antimony) was observed to have an amplitude $\sim 10(30)$ times smaller than the high-symmetry A_{1g} mode [12,17]. A density functional theory study has shown that the initial photoinduced driving force on the symmetry-preserving (A_{1g}) and symmetry-breaking (E_g) coherent modes of bismuth are comparable [32]. Therefore, the highly reduced amplitude of the E_g mode indicates that the E_g driving force is extremely short lived. Recent experimental work utilized a combination of optical pump-optical probe and continuous-wave (cw) Raman scattering to indirectly determine the lifetime of the E_g driving force in Bi and Sb as a function of temperature. The E_g force lifetime in bismuth (antimony) was found to vary from 13 ± 4 fs (17 ± 2 fs) at 10 K to 2 ± 0.4 fs (5.5 ± 0.5 fs) at room temperature [17]. It was suggested that the rapid, temperature-dependent relaxation of this force was due to the initial low-symmetry excited electron-hole plasma rapidly regaining full symmetry via electron-phonon scattering. A similar conclusion was reached in other experimental work [12], where the E_g driving force in bismuth was shown to have a decay time of ~ 4 fs at room temperature. A study of the coherent modes in topological insulator Bi_2Te_3 showed similar behavior of the symmetry-breaking E_g modes, whose relatively small amplitude compared with the fully symmetric A_{1g} modes was attributed to short-lived photoexcited electronic states with lifetimes ~ 10 fs [18]. A recent calculation [33] found the timescale for equilibration of L valley occupations in photoexcited silicon via electron-phonon scattering to be 180 fs, but did not consider the consequences for the generation of symmetry-breaking coherent atomic motion.

The group-V semimetals crystallize in the A7 rhombohedral structure, with 2 atoms per unit cell. One atom is at the origin and the other displaced a distance zc along the trigonal axis (c axis), which is represented by a dashed line in the inset of Fig. 1. The internal atomic displacement parameter z is highly sensitive to excitation of electrons to the conduction bands. This alters the equilibrium value of z and generates oscillations of the symmetry-preserving A_{1g} mode. In contrast, the symmetry-breaking E_g mode involves motion of the atoms perpendicular to the c axis and is thus not driven by the conventional DECP mechanism, which assumes occupations of excited electron states that preserve crystal symmetry. The E_g mode is driven by unbalanced occupation of symmetry-equivalent regions of the Brillouin zone following photoexcitation by a pump polarized perpendicular to the threefold axis of the crystal [17,32].

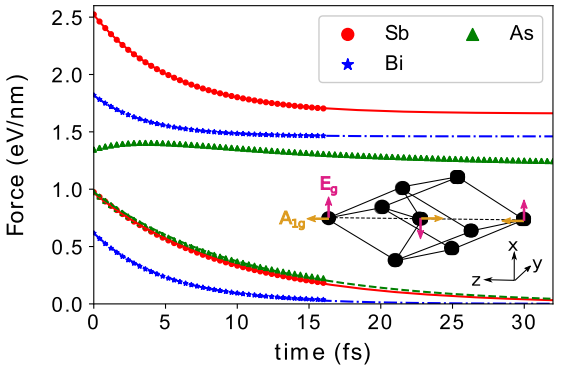

FIG. 1. The E_g and A_{1g} driving forces in Bi, Sb, and As as functions of time delay, following the absorption of 0.1 photons of energy 1.5 eV per unit cell. The three upper plots show the A_{1g} force, the three lower show the E_g force. The solid lines are fittings to the explicitly calculated data points. F_{E_g} is fit to a decaying exponential $F_{E_g}(t=0)\exp -t/\tau_{E_g}$ and $F_{A_{1g}}$ is fit to a decaying exponential plus a constant term: $F^1_{A_{1g}}\exp -t/\tau_{A_{1g}} + F^2_{A_{1g}}$ as discussed in the main text. Inset: The unit cell of the group-V semimetals. The green (blue) arrows indicate atomic motion corresponding to the E_g (A_{1g}) modes.

We compute electron states $|n\mathbf{k}\rangle$ with energy $\epsilon_{n\mathbf{k}}$ for band n at momenta $\mathbf{k}$, and phonon normal modes $\mathbf{e}^{\lambda}(\mathbf{q})$ with frequency $\omega_{\lambda\mathbf{q}}$ at momenta $\mathbf{q}$ on a uniform grid in the Brillouin zone and find the electron-phonon matrix elements, $g^{\lambda\mathbf{q}}_{\mathbf{k}nm}$ as defined in Ref. [34], on the same grid using DFPT [27]. These quantities are then interpolated to a finer grid using maximally localized Wannier functions [35]. We generate the initial nonequilibrium photoexcited distribution in the same manner as Ref. [32]. The excited electronic occupations are then evolved in time using electron-phonon rate equations [28–30]:

$$\frac{\partial f_{n\mathbf{k}}}{\partial t} = \sum_{m,\mathbf{q},\lambda,\xi} [R^{\xi}_{\lambda}(m\mathbf{k}+\mathbf{q}, n\mathbf{k}) - R^{\xi}_{\lambda}(n\mathbf{k}, m\mathbf{k}+\mathbf{q})], \quad (1)$$

$$\frac{\partial n_{\mathbf{q}\lambda}}{\partial t} = \sum_{\mathbf{k},n,m} [R^{+}_{\lambda}(m\mathbf{k}+\mathbf{q}, n\mathbf{k}) - R^{-}_{\lambda}(n\mathbf{k}, m\mathbf{k}+\mathbf{q})], \quad (2)$$

where $\xi =$ phonon emission (+) or phonon absorption (−), $f_{n\mathbf{k}}$ ($f_{m\mathbf{k}+\mathbf{q}}$) is the occupation of electronic state $|n\mathbf{k}\rangle$ ($|m\mathbf{k}+\mathbf{q}\rangle$), $n_{\mathbf{q},\lambda}$ are the phonon occupations for branch λ, and R^{ξ}_{λ} are the electron-phonon scattering rates defined by Fermi's golden rule,

$$R^{\pm}_{\lambda}(n\mathbf{k}, m\mathbf{k}+\mathbf{q}) = \frac{1}{N}\frac{1}{\omega_{\lambda\mathbf{q}}} |g^{\lambda\mathbf{q}}_{\mathbf{k}nm}|^2 f_{n\mathbf{k}}(1 - f_{m\mathbf{k}+\mathbf{q}}) \left(n_{\lambda\mathbf{q}} + \frac{1}{2} \pm \frac{1}{2}\right) \times \delta(\varepsilon_{m\mathbf{k}+\mathbf{q}} - \varepsilon_{n\mathbf{k}} \pm \omega_{\lambda\mathbf{q}}), \quad (3)$$

where N is the number of wave vectors $\mathbf{k}$ (or $\mathbf{q}$) in the uniform Brillouin zone grid, $\omega_{\mathbf{q}\lambda}$ are the phonon frequencies, and $\delta(\varepsilon_{m\mathbf{k}+\mathbf{q}} - \varepsilon_{n\mathbf{k}} \pm \omega_{\lambda\mathbf{q}})$ are the energy conserving delta functions for emission and absorption of a phonon. Finite lifetimes give the electronic states a Lorentzian line shape in energy and the energy conservation delta function broadens to a Lorentzian whose width is the sum of the linewidths of the initial and final state in the scattering process [36]:

$$P^{\pm} = \frac{\Im\Sigma_{m\mathbf{k}+\mathbf{q}} + \Im\Sigma_{n\mathbf{k}}}{[\Delta\varepsilon^{nm}_{\mathbf{k},\mathbf{k}+\mathbf{q}} \pm \omega_{\lambda\mathbf{q}}]^2 + [\Im\Sigma_{m\mathbf{k}+\mathbf{q}} + \Im\Sigma_{n\mathbf{k}}]^2}, \quad (4)$$

where $\Delta\varepsilon^{nm}_{\mathbf{k},\mathbf{k}+\mathbf{q}} = \varepsilon_{m\mathbf{k}+\mathbf{q}} - \varepsilon_{n\mathbf{k}}$ and $\Im\Sigma_{n\mathbf{k}}$ is the imaginary part of the electron self-energy for state $|n\mathbf{k}\rangle$. It is temperature dependent and related to the equilibrium lifetime of the state via $1/\tau_{n\mathbf{k}}(T) = 2\Im\Sigma_{n\mathbf{k}}(T)/\hbar$ [34] [37]. This brings our rate equations into agreement with the completed-collisions limit of the Kadanoff-Baym equations [33]. For reasons of numerical efficiency, we replace these Lorentzians with Gaussians of the same width.

The atomic force $\boldsymbol{F}_{\boldsymbol{\alpha}}$ on atom α in the unit cell is computed at each time step using the diagonal part of the electron-phonon matrix [38]:

$$\boldsymbol{F}_{\alpha} = -\frac{1}{N}\sum_{n,\mathbf{k}} \Delta f_{n\mathbf{k}} \langle n\mathbf{k}|\nabla_{\boldsymbol{\tau}_{\boldsymbol{\alpha}}}\hat{H}|n\mathbf{k}\rangle, \quad (5)$$

where $\Delta f_{n\mathbf{k}} = f_{n\mathbf{k}} - f^0_{n\mathbf{k}}$ is the change in occupation of state $|n\mathbf{k}\rangle$ from its equilibrium value and $\boldsymbol{\tau}_{\boldsymbol{\alpha}}$ is the displacement of atom α from equilibrium [41].

The time evolution of both the E_g and the A_{1g} driving forces are shown in Fig. 1, demonstrating that the E_g force exponentially decays to zero, as expected, while the A_{1g} force undergoes a more complex time evolution. In Bi and Sb, the A_{1g} force undergoes a partial decay from its initial value to a nonzero constant. In As, the A_{1g} force increases slightly before decaying to a nonzero constant. This is not surprising, since the evolution of the A_{1g} force depends on the precise distribution of photoexcited electrons. In fact, at some other photon energies, the evolution of the A_{1g} forces in Bi and Sb also depart from purely exponential behavior. The final values of the A_{1g} forces in Bi and Sb are obtained by fitting the calculated time-dependent values to a decaying exponential plus a constant term, as explained in the caption of Fig. 1. In As, we extract the final A_{1g} force by fitting the same function to the tail of the calculated values. In Table I, we see that the final A_{1g} forces in all three materials are slightly higher than that which would be obtained in constrained DFT (CDFT) by assuming a hot thermal distribution of electrons and holes, with different chemical potentials [42]. The A_{1g} force will eventually relax to 0 when the excited electronic occupations return to equilibrium, i.e., $\Delta f_{n\mathbf{k}} = 0$, as indicated by Eq. (5).

TABLE I. Comparison of initial (F^i_{A1g}) and final A_{1g} force (F^f_{A1g}) with those obtained in a two-chemical potential CDFT calculation ($F^{2\mu}_{A1g}$) [42]. The forces are computed assuming an absorbed fluence of 0.1 photons of energy 1.5 eV per unit cell.

Material	F^i_{A1g} (eV/nm)	F^f_{A1g} (eV/nm)	$F^{2\mu}_{A1g}$ (eV/nm)
Bismuth	1.82	1.46	1.34
Antimony	2.52	1.66	1.38
Arsenic	1.35	1.21	1.13

However, this process occurs on much longer timescales (>10 ps) [44] and is beyond the scope of this work.

Li *et al.* [17] determined the E_g force lifetime indirectly, by comparing the ratio of the E_g to A_{1g} mode amplitude in an optical pump-optical probe experiment with cross sections obtained in a cw Raman scattering experiment. The experimental E_g force lifetimes in Ref. [17] were derived, assuming that the A_{1g} force does not change over the duration of the pump pulse (∼70 fs). However, our calculations show a decay of the A_{1g} force from $F_0 \to sF_0$ in much less than 70 fs for Bi ($s \sim 0.80$) and Sb ($s \sim 0.65$), as shown in Fig. 1. We adjust the experimental analysis in Ref. [17] to account for this partial decay. See Supplemental Material for the full details [38]. This allows us to make a quantitative comparison between our calculated E_g force lifetimes and the experimental ones.

In Fig. 2, the calculated and experimental E_g force lifetime are shown as functions of temperature for Bi and

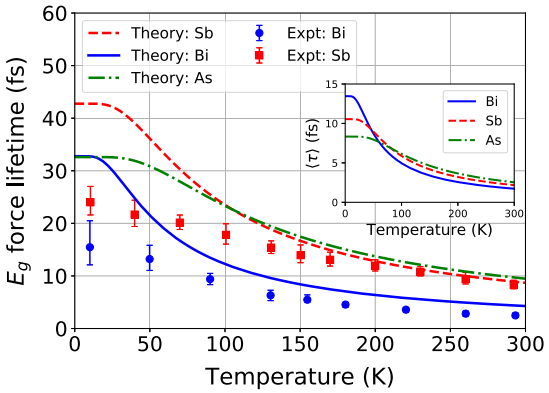

FIG. 2. Lifetime of driving force on E_g mode as a function of lattice temperature for Bi, Sb, and As for a pump photon energy of 1.5 eV. The curves are theoretical results, the points are the experimentally inferred values [17] rederived taking into account the partial decay of the A_{1g} force. Inset: the average lifetime of states within the excited electron-hole plasma, as defined in Eq. (6). Both $\langle\tau\rangle$ and τ_{E_g} were computed for 16 temperatures in the interval [0.1, 300] K and fitted with the function $f(T) = f(0)/[1 + 2n_B(T, \Omega_0)]$, where $n_B(T, \Omega_0)$ is the Bose-Einstein occupation number for a mode frequency Ω_0 at temperature T and Ω_0 is a fitting parameter: $\hbar\Omega_0(\mathrm{Bi}) \approx 6.8$ meV, $\hbar\Omega_0(\mathrm{Sb}) \approx 10.7$ meV, and $\hbar\Omega_0(\mathrm{As}) \approx 15.5$ meV.

Sb [45], and only the calculated values for As, where no experimental measurements are available. The pump pulse photon energy in the calculations is 1.5 eV, as in the experiment in Ref. [17].

The agreement between theory and experiment is good. In particular, the calculated E_g force relaxation rate in antimony differs from experiment by a constant scattering rate of $\Gamma \sim 12.5$ ps^{-1} [38], consistent with a temperature-independent scattering mechanism due to static imperfections in the sample, such as impurities or grain boundaries. The calculated relaxation rate in bismuth differs from experiment by a roughly uniform factor of ~1.5. This small discrepancy could be due to some additional scattering mechanism not considered here, such as electron-electron scattering. However, given the challenging nature of the experiment, the agreement is good and confirms that electron-phonon scattering is the dominant relaxation mechanism for the E_g driving force in both materials. Calculations of the E_g force lifetime keeping the phonon populations fixed at their initial values differ from the full calculations by less than 1%, indicating that evolution of the phonon populations is not important for the relaxation of the E_g force. Thus the E_g force relaxation is primarily due to coupling between the excited electron-hole plasma and the preexisting thermal disorder present at the time of photoexcitation.

The inset of Fig. 2 shows the average lifetime of states within the excited electron-hole plasma due to electron-phonon coupling, which we define

$$\frac{1}{\langle\tau(T)\rangle} = \frac{\sum_{n\mathbf{k}\in \mathrm{vb}} \gamma_{n\mathbf{k}}(T)(1-f_{n\mathbf{k}})}{\sum_{n\mathbf{k}\in \mathrm{vb}} (1-f_{n\mathbf{k}})} + \frac{\sum_{n\mathbf{k}\in \mathrm{cb}} \gamma_{n\mathbf{k}}(T) f_{n\mathbf{k}}}{\sum_{n\mathbf{k}\in \mathrm{cb}} f_{n\mathbf{k}}}, \qquad (6)$$

where $\gamma_{n\mathbf{k}}$ are the equilibrium inverse relaxation times of the electronic states $|n\mathbf{k}\rangle$ [48] and $f_{n\mathbf{k}}$ are the initial photoexcited electronic occupations following absorption of 1.5 eV photons. We see that the average lifetime of the electron-hole plasma is similar to, but less than the E_g force lifetime in all three materials, since not all electron-phonon scattering events degrade the E_g force, but all relax the states within the electron-hole plasma. This could be useful in more structurally complex systems where a full simulation of atomic force decay would be computationally demanding. A large value of $\langle\tau\rangle$ means that the excited electronic states have long lifetimes, which could potentially facilitate the generation of long lived symmetry-breaking atomic forces. We further note that the temperature dependence of the E_g force lifetime is very similar to that of $\langle\tau\rangle$. Thus, if we compute the lifetime of the E_g force at low temperature, we can estimate $\tau_{E_g}(T)$ by computing $\langle\tau(T)\rangle$, which is computationally much less demanding. In more structurally complex materials, where a full simulation of the force decay might be very difficult, $\langle\tau\rangle$ should provide a reasonable approximation of the lifetime of symmetry-breaking atomic driving forces.

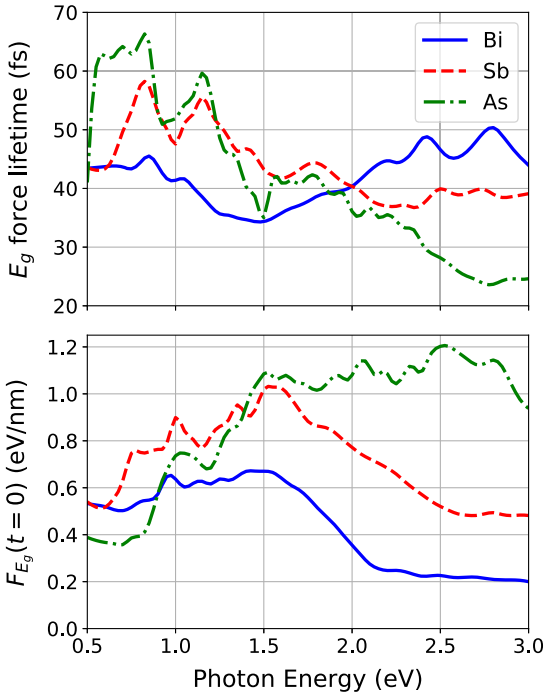

FIG. 3. Upper: Low temperature (0.1 K) driving force lifetime of the E_g photoexcited force in Bi, Sb, and As, as functions of the pump photon energy. Lower: Initial E_g driving force as functions of pump photon energy, assuming 0.1 photons absorbed per unit cell.

The similarity between $\langle\tau\rangle$ and the lifetime of the E_g force underlines the importance of the coupling between the excited electron-hole plasma and the continuum of thermal vibrations in determining the behavior of symmetry-breaking atomic driving forces. This is in contrast to the A_{1g} driving force, which decays to a value similar to the force we would obtain by assuming two separate thermal distributions for the photoexcited electrons and holes, on timescales less than 100 fs (as shown in Fig. 1 and Table I). This underlines that the dynamics affecting symmetry-breaking forces are quite different to those determining symmetry-preserving forces.

In Fig. 3, we show that both the initial E_g force and the E_g force lifetime vary substantially with the pump photon energy in all three materials [49]. The amplitude of the E_g mode is proportional to the product $\tau_{E_g} F_{E_g}(t=0)$, for a given number of photons absorbed per unit cell [50]. Within the energy range considered, this indicates that bismuth should be pumped with photons of energy ~0.9 eV, antimony with photons of energy in the interval [1.0, 1.5] eV, and arsenic with photons of energy in the interval [1.0, 2.5] eV to maximize the E_g mode amplitude. In other materials, choosing a photon energy which maximizes $\tau_{E_g} F_{E_g}(t=0)$ would enable us to increase

the amplitude of symmetry-breaking coherent modes, which could permit investigation into the possibility of inducing structural phase transitions that lower crystal symmetry [12].

In conclusion, we have presented a first principles method for calculating the generation and relaxation of low-symmetry photoinduced forces, which goes beyond conventional TDDFT approaches by explicitly considering coupling between the excited electron-hole plasma and the continuum of thermal vibrations, enabling us to accurately describe the ultrafast excitation and relaxation of the symmetry-breaking E_g driving force in Bi, Sb, and As. We have defined a nonequilibrium average lifetime of states within the electron-hole plasma and shown that it provides a crude indication of the E_g force lifetime and has the same temperature dependence as the E_g force lifetime in all three materials, making it a computationally useful diagnostic for the lifetime of low-symmetry photoinduced forces in more structurally complex materials. We have demonstrated that the lifetimes of the E_g forces in Bi, Sb, and As vary substantially with the photon energy of the pump pulse, and suggest that similar effects would occur in other materials, providing a path to generating larger amplitude symmetry-breaking atomic motion by suitable choice of pump photon energy.

This work was supported financially by Science Foundation Ireland Grant No. 12/IA/1601 and the Irish Research Council Grant No. GOIPG/2015/2784. We acknowledge the Irish Centre for High-End Computing (ICHEC) for the provision of computational facilities.

[1] J. Stähler, U. Bovensiepen, M. Meyer, and M. Wolf, Chem. Soc. Rev. **37**, 2180 (2008).
[2] S. Wall, S. Yang, L. Vidas, M. Chollet, J. M. Glownia, M. Kozina, T. Katayama, T. Henighan, M. Jiang, T. A. Miller *et al.*, Science **362**, 572 (2018).
[3] S. W. Teitelbaum, T. Shin, J. W. Wolfson, Y.-H. Cheng, I. J. Porter, M. Kandyla, and K. A. Nelson, Phys. Rev. X **8**, 031081 (2018).
[4] M. Rini, A. Cavalleri, R. W. Schoenlein, R. López, L. C. Feldman, R. F. Haglund, L. A. Boatner, and T. E. Haynes, Opt. Lett. **30**, 558 (2005).
[5] Z. Li, Y. Chen, and C. Burda, J. Phys. Chem. C **123**, 3255 (2019).
[6] M. Salinga, B. Kersting, I. Ronneberger, V. P. Jonnalagadda, X. T. Vu, M. Le Gallo, I. Giannopoulos, O. Cojocaru-Mirédin, R. Mazzarello, and A. Sebastian, Nat. Mater. **17**, 681 (2018).
[7] E. Kuramochi and M. Notomi, Nat. Photonics **9**, 712 (2015).
[8] J. Shah, *Ultrafast Spectroscopy of Semiconductors and Semiconductor Nanostructures* (Springer, Berlin, 1996).
[9] D. Rudolf, C. La-O-Vorakiat, M. Battiato, R. Adam, J. M. Shaw, E. Turgut, P. Maldonado, S. Mathias, P. Grychtol, H. T. Nembach *et al.*, Nat. Commun. **3**, 1037 (2012).
[10] M. Weis, K. Balin, R. Rapacz, A. Nowak, M. Lejman, J. Szade, and P. Ruello, Phys. Rev. B **92**, 014301 (2015).
[11] D. M. Fritz, D. A. Reis *et al.*, Science **315**, 633 (2007).
[12] S. L. Johnson, P. Beaud, E. Möhr-Vorobeva, A. Caviezel, G. Ingold, and C. J. Milne, Phys. Rev. B **87**, 054301 (2013).
[13] M. Trigo, M. Fuchs, J. Chen, M. P. Jiang, M. Cammarata *et al.*, Nat. Phys. **9**, 790 (2013).
[14] A. Stolow, A. E. Bragg, and D. M. Neumark, Chem. Rev. **104**, 1719 (2004).
[15] F. Schmitt, P. S. Kirchmann, U. Bovensiepen, R. G. Moore, L. Rettig, M. Krenz, J. H. Chu, N. Ru, L. Perfetti, D. H. Lu, M. Wolf, I. R. Fisher, and Z. X. Shen, Science **321**, 1649 (2008).
[16] B. Mansart, M. J. G. Cottet, T. J. Penfold, S. B. Dugdale, R. Tediosi, M. Chergui, and F. Carbone, Proc. Natl. Acad. Sci. U.S.A. **109**, 5603 (2012).
[17] J. J. Li, J. Chen, D. A. Reis, S. Fahy, and R. Merlin, Phys. Rev. Lett. **110**, 047401 (2013).
[18] O. V. Misochko, A. A. Mel'nikov, S. V. Chekalin, and A. Y. Bykov, JETP Lett. **102**, 235 (2015).
[19] N. Kamaraju, S. Kumar, M. Anija, and A. K. Sood, Phys. Rev. B **82**, 195202 (2010).
[20] T. Huber, M. Ranke, A. Ferrer, L. Huber, and S. L. Johnson, Appl. Phys. Lett. **107**, 091107 (2015).
[21] T. E. Stevens, J. Kuhl, and R. Merlin, Phys. Rev. B **65**, 144304 (2002).
[22] G. A. Garrett, T. F. Albrecht, J. F. Whitaker, and R. Merlin, Phys. Rev. Lett. **77**, 3661 (1996).
[23] T. K. Cheng, J. Vidal, H. J. Zeiger, G. Dresselhaus, M. S. Dresselhaus, and E. P. Ippen, Appl. Phys. Lett. **59**, 1923 (1991).
[24] C. E. Crespo-Hernández, B. Cohen, P. M. Hare, and B. Kohler, Chem. Rev. **104**, 1977 (2004).
[25] H. J. Zeiger, J. Vidal, T. K. Cheng, E. P. Ippen, G. Dresselhaus, and M. S. Dresselhaus, Phys. Rev. B **45**, 768 (1992).
[26] R. Merlin, Solid State Commun. **102**, 207 (1997).
[27] S. Baroni, S. De Gironcoli, A. Dal Corso, and P. Giannozzi, Rev. Mod. Phys. **73**, 515 (2001).
[28] O. Madelung, *Introduction to Solid-State Theory* (Springer, Berlin, 1978), pp. 187–193.
[29] P. Maldonado, K. Carva, M. Flammer, and P. M. Oppeneer, Phys. Rev. B **96**, 174439 (2017).
[30] S. Sadasivam, M. K. Y. Chan, and P. Darancet, Phys. Rev. Lett. **119**, 136602 (2017).
[31] E. Runge and E. K. U. Gross, Phys. Rev. Lett. **52**, 997 (1984).
[32] É. D. Murray and S. Fahy, Phys. Rev. Lett. **114**, 055502 (2015).
[33] D. Sangalli and A. Marini, Europhys. Lett. **110**, 47004 (2015).
[34] F. Giustino, Rev. Mod. Phys. **89**, 015003 (2017).
[35] N. Marzari, A. A. Mostofi, J. R. Yates, I. Souza, and D. Vanderbilt, Rev. Mod. Phys. **84**, 1419 (2012).
[36] A. Marini, J. Phys. Conf. Ser. **427**, 012003 (2013).
[37] In practice, we calculate $\Im\Sigma_{n\mathbf{k}}$ by replacing the energy conserving delta function with a Gaussian. However, the calculated E_g force lifetimes are insensitive to the width of this Gaussian [38].
[38] See Supplemental Material at http://link.aps.org/supplemental/10.1103/PhysRevLett.123.087401 for details on convergence of calculations, Wannier interpolation, rederivation of experimental E_g force lifetimes from Ref. [17] accounting for the partial A_{1g} force decay and a derivation of Eq. (5). This includes Refs. [39] and [40].

[39] R. P. Feynman, Phys. Rev. **56**, 340 (1939).
[40] R. M. Martin, *Electronic Structure: Basic Theory and Practical Methods* (Cambridge University Press, Cambridge, England, 2004).
[41] We have also computed the atomic forces self-consistently within the framework of CDFT [42] using the ABINIT package [43]. We find that the E_g force computed both ways agree very well, so we use the approach in Eq. (5) as it is more efficient. The A_{1g} force depends more delicately on the exact values of the equilibrium electronic occupations, $f^0_{n\mathbf{k}}$, so is more accurately computed using CDFT.
[42] P. Tangney and S. Fahy, Phys. Rev. Lett. **82**, 4340 (1999).
[43] X. Gonze *et al.*, Comput. Phys. Commun. **180**, 2582 (2009).
[44] Y. M. Sheu, Y. J. Chien, C. Uher, S. Fahy, and D. A. Reis, Phys. Rev. B **87**, 075429 (2013).
[45] Electron energies, phonon frequencies, and electron-phonon matrix elements were computed on a $6 \times 6 \times 6$ grid using QUANTUM ESPRESSO [46] and interpolated to a $14 \times 14 \times 14$ grid using the EPW code [47].
[46] P. Giannozzi *et al.*, J. Phys. Condens. Matter **21**, 395502 (2009).
[47] S. Poncé, E. Margine, C. Verdi, and F. Giustino, Comput. Phys. Commun. **209**, 116 (2016).
[48] G. Grimvall, *The Electron-Phonon Interaction in Metals* (North-Holland, Amsterdam, 1981).
[49] These calculations were performed on a $16 \times 16 \times 16$ grid.
[50] A more exact expression would be $A_{E_g} \propto F_{E_g}(t=0)/\sqrt{1+(1/\tau^2_{E_g}\Omega^2_{E_g})}$, which reduces to $A_{E_g} \propto \tau_{E_g} F_{E_g}(t=0)$ in the limit where $1/\tau^2_{E_g}\Omega^2_{E_g} \gg 1$.